

Ab Initio Potential Energy Surface for NaCl–H₂ with Correct Long-Range Behavior

Priyanka Pandey, Chen Qu, Apurba Nandi, Qi Yu, Paul L. Houston, Riccardo Conte, and Joel M. Bowman*



Cite This: *J. Phys. Chem. A* 2024, 128, 902–908



Read Online

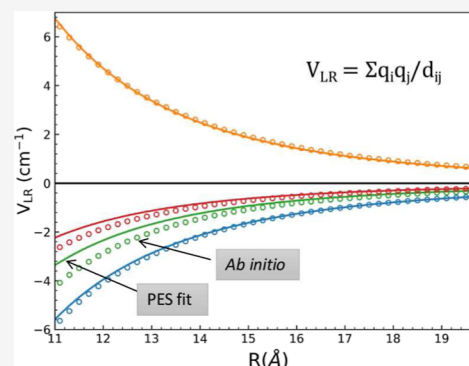
ACCESS |

Metrics & More

Article Recommendations

Supporting Information

ABSTRACT: We report a full dimensional ab initio potential energy surface for NaCl–H₂ based on precise fitting of a large data set of CCSD(T)/aug-cc-pVTZ energies. A major goal of this fit is to describe the very long-range interaction accurately. This is done in this instance via the dipole–quadrupole interaction. The NaCl dipole and the H₂ quadrupole are available through previous works over a large range of internuclear distances. We use these to obtain exact effect charges on each atom. Diffusion Monte Carlo calculations are done for the ground vibrational state using the new potential.



1. INTRODUCTION

Molecular hydrogen is the fundamental component in the interstellar medium and is prevalent in most interstellar environments. Collisions involving molecular hydrogen interacting with itself and other rotationally and vibrationally excited molecules are the essential components of astrophysics to understand the evolution of planetary gases.^{1,2} Since replicating the precise conditions of astrophysical environments in the laboratory is challenging, most collision studies involving molecular hydrogen and other molecules rely on quantum scattering calculations, necessitating an accurate understanding of the relevant interaction potential energy surface (PES). In recent years, researchers have addressed the potential energy surface of various systems involving molecular hydrogen, including H₂ + H₂,³ SiO₂–H₂,⁴ CN–H₂,⁵ CO–H₂,⁶ and others.^{7,8} Apart from these predominant molecules, the formation of molecules composed of elements with lower abundances also occurs. For instance, recently, sodium chloride has been discovered in Europa,⁹ in the disk around Orion Source I,¹⁰ as well as in other locations.^{11,12} Hence, the computation of a full-dimensional PES for the NaCl–H₂ system is required to understand the collisions between them.

Previously, experimental and theoretical studies have been conducted to investigate the behavior of H₂ on crystalline solid surfaces and in aqueous solutions of NaCl. For instance, Ewing, Heidberg, and others conducted multiple experiments to explore the adsorption of H₂ on annealed NaCl films and NaCl(110) using infrared (IR) spectroscopy^{13–16} and He atom scattering.¹⁷ Additionally, Monte Carlo simulations and perturbation theory calculations were utilized to investigate the

structure of monolayer and bilayer films of H₂ molecules adsorbed on NaCl(001) at different temperatures.¹⁸ Recently, Zhu et al. developed an accurate model of H₂ solubility in aqueous NaCl solution.¹⁹ To the best of our knowledge, no NaCl–H₂ PES exists addressing the interaction between NaCl and H₂.

The accuracy of the PES for many atom systems, including biomolecules, condensed matter, and macromolecules, depends on the precise depiction of both short-range and long-range interactions. Therefore, accurately describing the long-range interaction potential is crucial to PES calculation²⁰ and understanding phenomena such as molecular collisions,^{21,22} dispersion,²³ and extended charge transfer.^{24,25} To achieve this goal, modeling long-range interactions using electrostatic, induction, and dispersion components yields computationally efficient and precise results.²⁶

Describing long-range interactions is a challenge for the large class of atom-centered machine learning methods that use a strict cutoff for the interaction range to represent potentials.^{27,28} Quoting from Behler and co-workers in 2021, “Machine learning potentials...[that] rely on local properties... are unable to take global changes in the electronic structure into account, which result from long-range charge transfer or

Received: November 21, 2023

Revised: December 26, 2023

Accepted: January 4, 2024

Published: January 25, 2024



different charge states.²⁹ The authors then present ad hoc proposals to account for long-range interactions in their fourth-generation neural network approach. Namely, they include classical electrostatic interactions that are damped to zero in the short-range. This approach goes back to the origins of small molecule potentials³⁰ and more modern versions of it have been incorporated into global methods that do not use range cutoffs, e.g., permutationally invariant polynomial (PIP)-based potentials. Examples include the PIP potentials for CH_5^{+31} and $(\text{H}_2\text{O})_2^{32}$. While these do fit data in the long-range, it was also clear that when available, switching to accurate long-range interactions made sense. For example, for the 2-body interaction in a many-body expansion of the water potential q-AQUA, the long-range interaction is switched to the dipole–dipole interaction³³ using an accurate, flexible dipole moment surface.³⁴ In order to avoid “ripples” in the final PES, it is important to verify that the machine-learned (ML) PES overlaps the long-range analytical potential accurately in the region of the switch, as was done in q-AQUA.³³

In the absence of a high-quality long-range interaction for flexible monomers, we have utilized two component fits.⁴ One component is a precise fit to data in the short-range, and the second one is a fit to data in the long-range. In the example in ref 4 for $\text{SiO} + \text{H}_2$, the long-range data, i.e., CCSD(T) energies, extend to 11.1 Å. The RMS fitting error for the long-range data is 0.05 cm^{-1} . This level of precision is just not feasible for a single fit to the entire data set.

In this paper, we present a full-dimensional potential energy surface for the NaCl-H_2 system, including the correct long-range behavior. The structure of the paper is outlined as follows: Section 2 provides a detailed description of the theoretical and computational aspects, including ab initio calculations, the fitting procedure, long-range interaction, and DMC calculations. The results and properties of the fitted potential energy surface are discussed in Section 3, followed by the summary and conclusions in Section 4.

2. COMPUTATIONAL DETAILS

The interaction potential for the NaCl-H_2 system in the electronic ground state has been computed using electronic energies generated predominantly on a six dimensional grid defined in Jacobi coordinates $(r_1, r_2, R, \theta_1, \theta_2, \phi)$ as shown in Figure 1. In this context, R is the distance between the centers of mass of NaCl and H_2 , while r_1 and r_2 indicate the respective bond lengths of the NaCl and H_2 molecule. Furthermore, θ_1 and θ_2 depict in-plane orientation angles between r_1 and R , and r_2 and R , while ϕ is the out-of-plane dihedral angle. In the ab initio calculations, R is varied in the range of 2.6–12.6 Å, while the bond distances are within the intervals of $2.16 \text{ Å} \leq r_1 \leq$

2.66 and $0.50 \text{ Å} \leq r_2 \leq 1.15 \text{ Å}$. The angular coordinates are within the ranges of $0^\circ \leq \theta_1 \leq 360^\circ$ and $0^\circ \leq \theta_2(\phi) \leq 180^\circ$ where $\theta_1 = \theta_2 = 0^\circ$ corresponds to the collinear arrangement Na-Cl-H-H .

All electronic energy calculations were performed using the coupled-cluster method with single and double excitations and perturbative treatment of triple [CCSD(T)] using the MOLPRO suite of quantum chemistry software programs.^{35,36} The ab initio calculations employed an augmented correlation-consistent polarized valence triple- ζ basis set (aug-cc-pVTZ).³⁷

The NaCl-H_2 potential is given by the “plug and play” form, i.e., it is written as the sum of an interaction potential plus potentials for isolated NaCl and H_2 , as we have done for several potentials.^{4,38} NaCl and H_2 monomers were fit using the simple sum of powers of the Morse variables. Note that here we employed a straightforward 1-d fit for the NaCl and H_2 monomers at the CCSD(T)/aug-cc-pVTZ level (abbreviated below as aVTZ). However, users have the flexibility to provide any monomer potential. At each NaCl-H_2 configuration, the interaction energy is given by the electronic energy of the NaCl-H_2 minus the electronic energy of NaCl and the electronic energy of H_2 . Clearly, this interaction potential goes to zero asymptotically as NaCl and H_2 separate. For the previous analogous potential for SiO-H_2 , CCSD(T) energies were obtained for R as large as 11 Å such that the interaction potential is less than 1 cm^{-1} .⁴ Note that the long-range interaction for NaCl-H_2 is stronger than that for $\text{SiO} + \text{H}_2$. To obtain a precise fit to these small asymptotic interaction energies, the PES fit in the short range (V_{SR}) was joined with the analytical long-range interaction (V_{LR}) with a smooth switching function as follows

$$V = (1 - s_1)V_{\text{SR}} + s_1V_{\text{LR}} \quad (1)$$

where

$$s_1 = \begin{cases} 0 & (R < R_i) \\ 10b^3 - 15b^4 + 6b^5 & (R_i \leq R \leq R_f) \\ 1 & (R > R_f) \end{cases} \quad (2)$$

and $R_i = 10.0 \text{ Å}$, $R_f = 11.0 \text{ Å}$, and $b = (R - R_i)/(R_f - R_i)$. Note that the choice of switching range R_i and R_f was motivated by the intention to capture a region where the direct CCSD(T) interaction energies exhibit a strong agreement with the analytical dipole–quadrupole interaction.

A large data set of ab initio points was calculated at the CCSD(T) level and used to fit the short-range PES. The PES has been fitted in 6D using an invariant polynomial method.

$$V_{\text{SR}} = \sum_{n_1 \dots n_6} c_{n_1 \dots n_6} y_1^{n_1} y_6^{n_6} [y_2^{n_2} y_3^{n_3} y_4^{n_4} y_5^{n_5} + y_2^{n_3} y_3^{n_2} y_4^{n_5} y_5^{n_4}] \quad (3)$$

where $c_{n_1 \dots n_6}$ is the linear coefficient and y_i are the Morse variables of form $\exp(-d_i/\lambda)$. The parameter λ is subject to user specification, which is set to $3.0a_0$ for V_{SR} . The internuclear distances d_i are denoted as $d_1 = d_{\text{NaCl}}$, $d_2 = d_{\text{NaH}}$, $d_3 = d_{\text{NaH}}$, $d_4 = d_{\text{ClH}}$, $d_5 = d_{\text{ClH}}$, and $d_6 = d_{\text{HH}}$. The total polynomial order for the fits is 7 resulting in a total of 918 linear coefficients. These were obtained using standard linear least-squares, utilizing the MSA software 2.0,^{39,40} which extends the original code^{41,42} to produce and also incorporate gradients data.

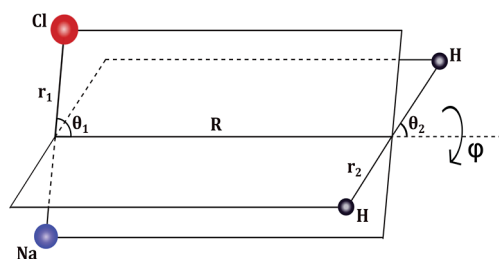


Figure 1. Six-dimensional Jacobi coordinates for the NaCl-H_2 system.

2.1. Long-Range Interaction between NaCl and H₂. The leading interaction potential between NaCl and H₂ in the long-range is given by the dipole–quadrupole interaction²⁶

$$V_{\text{LR}} = \frac{\mu\Theta}{R^4} \frac{3}{2} [\cos\theta_1(3\cos^2\theta_2 - 1) - \sin\theta_1 \sin 2\theta_2 \cos\phi] \quad (4)$$

where μ is the dipole moment of NaCl and Θ is the quadrupole moment of the H₂ molecule. Instead of using this directly, we use the equivalent expression employing Coulomb's law

$$V_{\text{LR}} = \sum \frac{q_i q_j}{d_{ij}} \quad (5)$$

where q_i are the point charges on NaCl and H₂ and d_{ij} are the corresponding distances between the charges on the different molecules. The charges on (q_{Na} and q_{Cl}) are determined using the dipole moment ($\vec{\mu} = q \cdot \vec{r}_1$) obtained from ref 43. The charges on the H₂ molecule are determined by noting that the quadrupole moment can be written as $-2q_{\text{H}}$ at the center of the molecule as shown in Figure 2. Therefore, the charges of

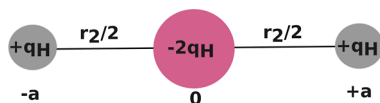


Figure 2. Electric quadrupole moment of the H₂ molecule.

the H₂ molecule at a given bond length are determined using the quadrupole moment obtained from ref 44. Using the given equation

$$\begin{aligned} \Theta &= \sum q_i x_i^2 = q_{\text{H}}(-a)^2 - 2q_{\text{H}}0 + q_{\text{H}}a^2 \\ &= 2q_{\text{H}}a^2 = q_{\text{H}}r_2^2/2 \end{aligned} \quad (6)$$

Figure 3 shows the variation of the NaCl dipole moment and the corresponding charge and the variation of the H₂ quadrupole moment and the effective charge with respect to the corresponding internuclear distances. We use eq 5 instead of eq 4 as the former is general and can be used for any term in the multipole expansion. We do note that other shorter range terms, such as the NaCl quadrupole and H₂ quadrupole interaction, are not considered since the NaCl quadrupole

moment as a function of the NaCl distance is not known. Further, as shown below, the leading dipole–quadrupole interaction does match up well to direct CCSD(T) interaction energies.

2.2. DMC. Unbiased diffusion Monte Carlo (DMC) calculations^{45–47} were performed to obtain the quantum zero point energy (ZPE) and wave function of the NaCl–H₂ system using the PES fit and to examine the quality of a PES in extended regions of the configuration space. The fundamental objective of DMC calculation is to solve the time-dependent Schrödinger wave equation in imaginary time τ . DMC calculations begin with an initial guess of the ground-state wave function represented by a population of $N(0)$ equally weighted Gaussian random walkers. Subsequently, these walkers diffuse randomly subject to the potential in imaginary time following a Gaussian distribution. Each walker has the possibility to persist (potentially giving birth to a new walker) or be eliminated; the population is regulated by birth-death processes, as described below

$$P_{\text{birth}} = \exp[-(E_i - E_r)\Delta\tau] - 1(E_i < E_r) \quad (7)$$

$$P_{\text{death}} = 1 - \exp[-(E_i - E_r)\Delta\tau](E_i > E_r) \quad (8)$$

where E_i is the energy of the i -th walker, E_r is the reference energy used to stabilize the diffusion system in its ground state, and $\Delta\tau$ is the step size in imaginary time. To keep the number of random walkers around the initial value $N(0)$, E_r is modified at the end of each time step as per the following equation.

$$E_r(\tau) = \langle V(\tau) \rangle - \alpha \frac{N(\tau) - N(0)}{N(0)} \quad (9)$$

where $N(\tau)$ is the number of walkers at the imaginary time step τ , $\langle V(\tau) \rangle$ is the average potential energy of all the alive walkers and α is the parameter that regulates the fluctuations in the number of walkers and the reference energy. The average of E_r over a sufficiently long time period provides an estimate of the ZPE. Here, we performed five DMC calculations, each with an imaginary time step of $\Delta\tau = 5$ au and $\alpha = 0.1$. For every DMC calculation, we propagated a set of 20,000 random walkers from the global minimum for 30,000 time steps (≈ 3.62 ps), out of which 20,000 steps are used to equilibrate the walkers, and the reference energies in the remaining 10,000 steps are used to compute the ZPE. The Cartesian coordinates

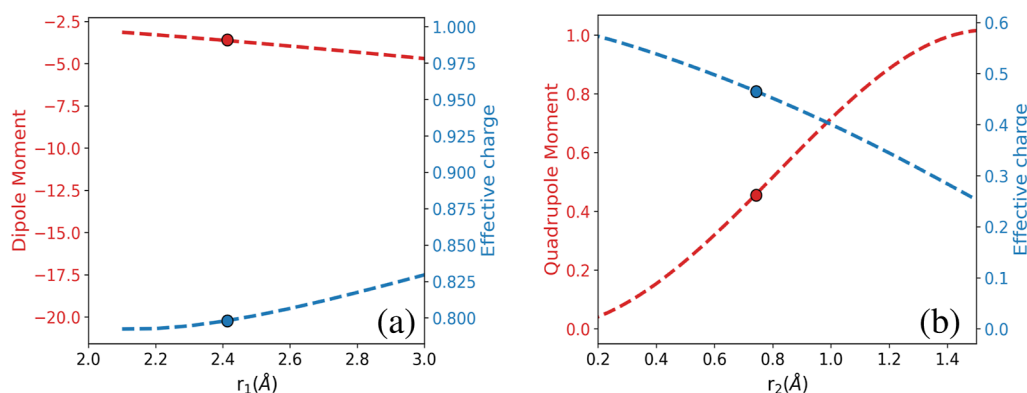


Figure 3. Dipole moment and calculated effective charge as a function of bond length (a) dipole moment and calculated effective charge for NaCl, and (b) quadrupole moment and calculated effective charge for H₂ molecule, with circles denoting the values at the equilibrium bond lengths. The dipole moment and quadrupole moment data are taken from refs 43 and 44.

of the walkers at the last ten steps were recorded, and their interatomic distances were determined.

3. RESULTS AND DISCUSSION

3.1. Precision of the Fits. The potential energy surfaces are fitted using the ab initio data, with a cut-off based on the maximum interaction energy. The precision of the PES fits was determined by calculating the root-mean-square (RMS) fitting errors as a function of the maximum interaction energy. In this work, we choose two interaction energy cut-offs of 20,000 and 2000 cm^{-1} as shown in Table 1. The RMS fitting errors in the

Table 1. RMS Fitting Error of Two PES Fits as a Function of the Maximum Energy Cut-Off^a

	V_{max}	RMS	data points
PES I	20,000	1.42	281,031
PES II	2000	1.23	241,155

^aEnergies are in cm^{-1} .

short-range fit are 1.42 cm^{-1} for PES I and 1.23 cm^{-1} for PES II. Note that our emphasis is on sampling the ab initio interaction energies essential for achieving an accurate fit. Although opting for an interaction energy range up to 2000 cm^{-1} is a suitable choice, computing additional points in the higher energy range, up to 20,000 cm^{-1} , is done for the completeness and to prevent the holes in the PES. Correlation plots are given for the two fits in Figure 4. As seen, there is nearly perfect correlation for both fits over the respective ranges of energies.

Table 2 presents the optimized geometrical structure and dissociation energy of the minimum for the PES fits with zero at the relaxed isolated NaCl and H_2 asymptote, comparing it with the MOLPRO calculated CCSD(T)/aVTZ optimized structures. Hereafter, PES refers to PES I. The global minimum is not for the T-shaped structure, and evidently this indicates that “chemical” effects beyond electrostatics are responsible for the global minimum. It might be interesting for those with more expertise than we have to analyze the source(s) responsible for this structure.

In Figure 5, several 1D cuts for the interaction energy between NaCl– H_2 are shown at different (θ_1 , θ_2 , ϕ) values from PES and are compared with the ab initio calculations

Table 2. Optimized Structures of NaCl– H_2 and Dissociation Energies of D_e (cm^{-1})^a

	CCSD(T)/aVTZ	PES I	PES II
r_1	2.4214	2.4214	2.4208
r_2	0.7497	0.7488	0.7487
R	2.7931	2.8400	2.8521
θ_1	113.9	114.6	115.4
θ_2	42.8	43.7	44.4
ϕ	180.0	180.0	180.0
D_e	632	646	642

^aDistances are in Å and angles are in degrees.

using the aVTZ basis sets. The bond distances of NaCl and H_2 are fixed at their equilibrium values, $r_1 = 2.413$ Å and $r_2 = 0.743$ Å for Figure 5a–c, whereas for Figure 5d, bond lengths are fixed to the values obtained from the optimized minimum geometry listed in Table 2. As seen, over the large range shown, there is excellent agreement between direct CCSD(T) energies and the PES, including in the long-range, R greater than 11 Å where the PES is given by the analytical dipole–quadrupole interaction. Note in panel (b) there is a small sudden variation in the PES energy at 10 Å where the switching to the analytical interaction begins. This is actually due to a correction to the PES that slightly underestimates the ab initio energies between around 8–10 Å. The switch restores excellent agreement with the ab initio energies.

Figure 6 shows the potential energy cut as a function of ϕ . All other coordinates are fixed in the NaCl– H_2 equilibrium configuration. As seen, there is a large energy change of roughly 1400 cm^{-1} , suggesting that the complex will maintain a mostly planar configuration.

3.2. Long-Range Interaction. A close examination of the dipole–quadrupole interaction is shown in Figure 7, along with direct CCSD(T) energies. As seen, the maximum deviation of the long-range interaction from the direct CCSD(T) energies is less than 1 cm^{-1} for $R = 11$ Å, which becomes almost exact with a further increase in R .

3.3. Zero-Point Wave Function. Next, we present results from the DMC calculations. When we conducted the unconstrained DMC, the PES was found to be “hole-free”, meaning that the PES does not contain any configurations with unphysical negative energies. The average ZPE obtained from

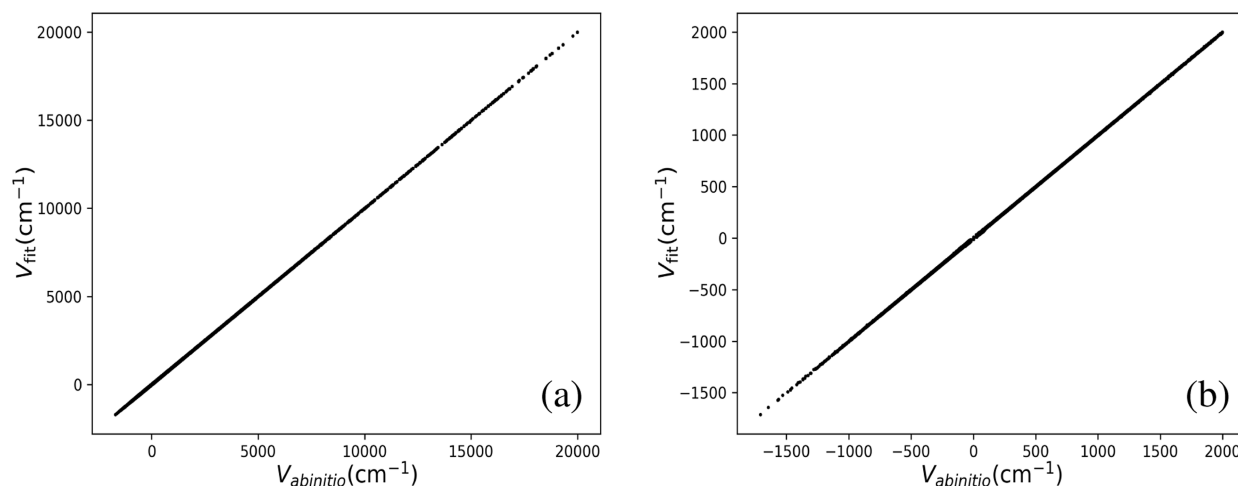


Figure 4. Correlation between fitted and ab initio CCSD(T)/aVTZ interaction energy for the energy cut-off of (a) 20,000, and (b) 2000 cm^{-1} .

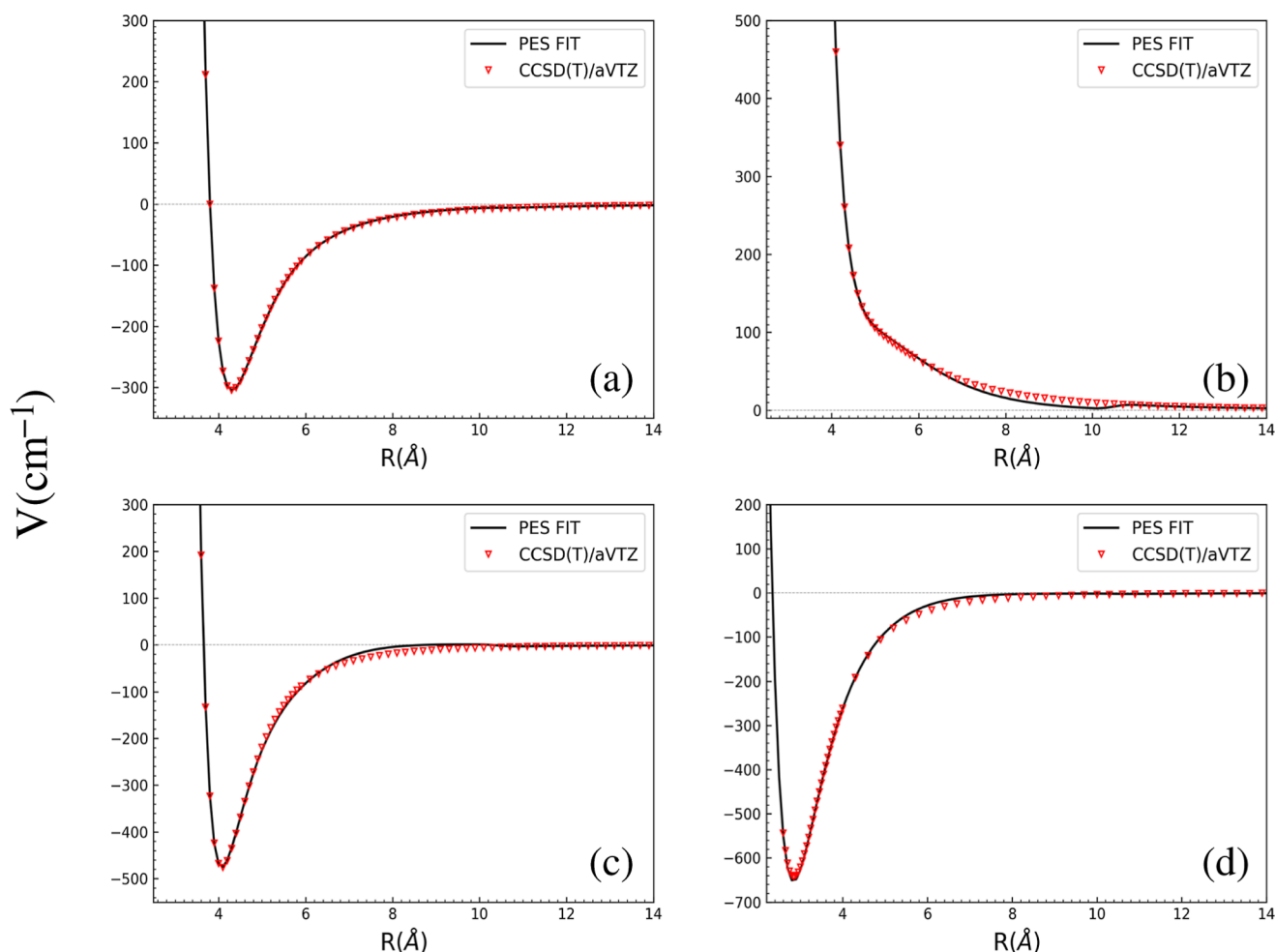


Figure 5. Comparison of several 1D cuts for the interaction energy between NaCl–H₂ as a function of internuclear distance R for various sets of $(\theta_1, \theta_2, \phi)$: (a) (0, 0, 0), (b) (180, 0, 0), (c) (180, 90, 0), and (d) (114.6, 43.7, 180).

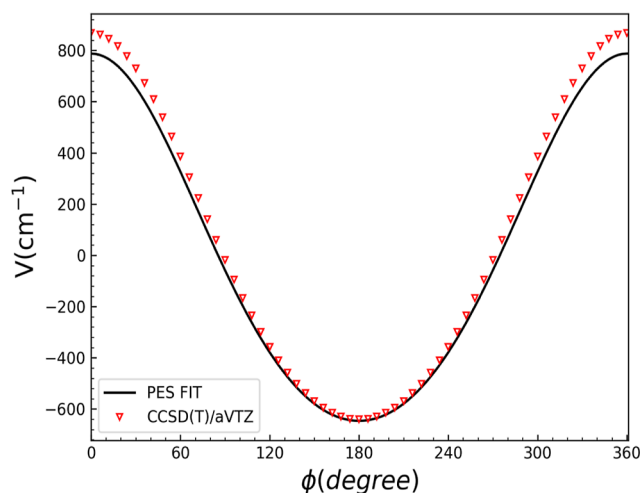


Figure 6. Potential energy cut of NaCl–H₂ as a function of ϕ .

five independent DMC simulations using the PES is $2778.16 \pm 1.72 \text{ cm}^{-1}$. Figure 8 shows histograms of the wave function vs the NaCl and H₂ internuclear distances, r_1 and r_2 , respectively, and R . As seen, the results for r_1 and r_2 closely resemble harmonic oscillator wave functions for the ground state. For R , where the motion is strongly anharmonic, the wave function

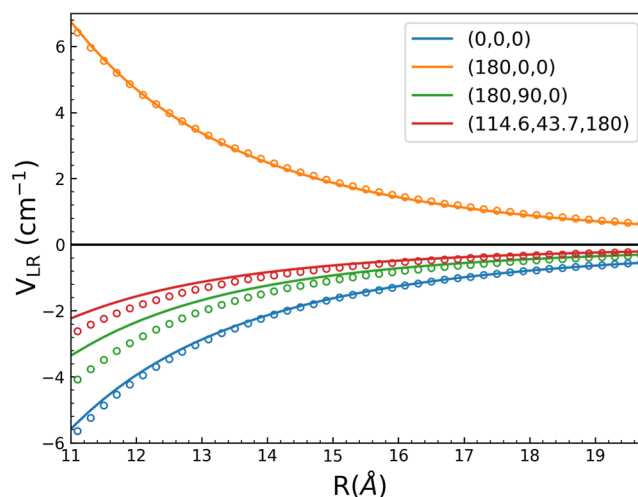


Figure 7. Long-range dipole–quadrupole interaction (solid lines) and corresponding ab initio energies (open circles) vs R for indicated $(\theta_1, \theta_2, \phi)$ sets.

displays an asymmetry which has more amplitude at large R -values than at small values.

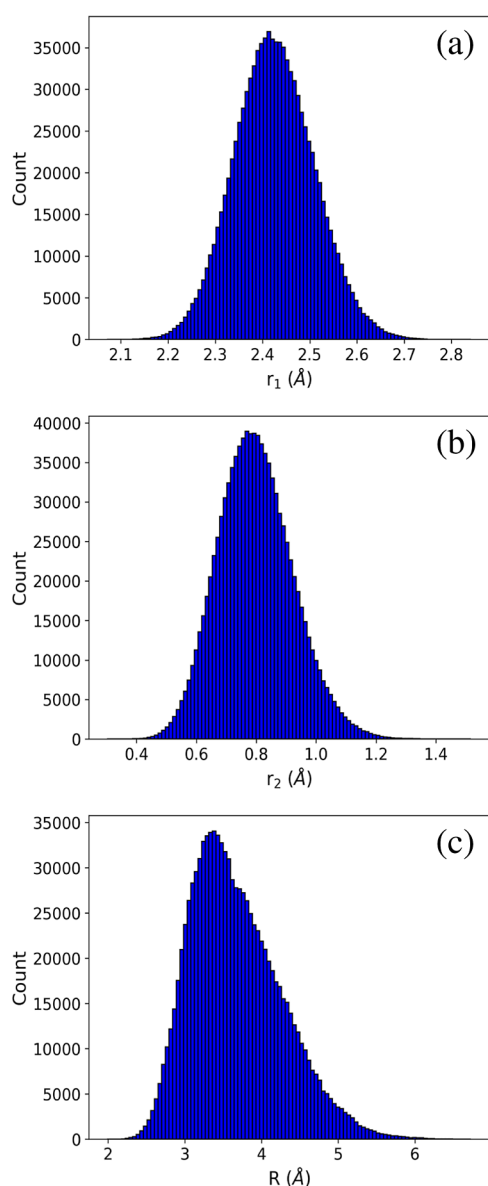


Figure 8. Histogram of cuts of the ground state DMC wave function vs the NaCl and H₂ internuclear distances, r_1 and r_2 , respectively, and R .

4. SUMMARY AND CONCLUSIONS

We reported a new potential energy surface for NaCl + H₂ from precise fitting of thousands of CCSD(T)/aug-cc-pVTZ energies. This PES is notable, as it is extended to infinite separation of NaCl and H₂ by means of an accurate dipole–quadrupole interaction for the flexible monomers. The PES is expressed as the sum of an interaction potential plus flexible monomer potentials, using the “plug and play” strategy adopted previously.³⁸

The electronic energies can be accessed at ref 48 and the PES is available as [Supporting Information](#).

■ ASSOCIATED CONTENT

SI Supporting Information

The Supporting Information is available free of charge at <https://pubs.acs.org/doi/10.1021/acs.jpca.3c07687>

The potential energy surface is supplied as Supporting Information (ZIP)

■ AUTHOR INFORMATION

Corresponding Author

Joel M. Bowman – Department of Chemistry and Cherry L. Emerson Center for Scientific Computation, Emory University, Atlanta, Georgia 30322, United States; orcid.org/0000-0001-9692-2672; Email: jmbowma@emory.edu

Authors

Priyanka Pandey – Department of Chemistry and Cherry L. Emerson Center for Scientific Computation, Emory University, Atlanta, Georgia 30322, United States; orcid.org/0000-0002-6930-792X

Chen Qu – Independent Researcher, Toronto ON M9B 0E3, Canada

Apurba Nandi – Department of Chemistry and Cherry L. Emerson Center for Scientific Computation, Emory University, Atlanta, Georgia 30322, United States; Department of Physics and Materials Science, University of Luxembourg, Luxembourg City L-1511, Luxembourg; orcid.org/0000-0002-6191-5584

Qi Yu – Department of Chemistry and Cherry L. Emerson Center for Scientific Computation, Emory University, Atlanta, Georgia 30322, United States; orcid.org/0000-0002-2030-0671

Paul L. Houston – Department of Chemistry and Chemical Biology, Cornell University, Ithaca, New York 14853, United States; Department of Chemistry and Biochemistry, Georgia Institute of Technology, Atlanta, Georgia 30332, United States; orcid.org/0000-0003-2566-9539

Riccardo Conte – Dipartimento di Chimica, Università Degli Studi di Milano, Milano 20133, Italy; orcid.org/0000-0003-3026-3875

Complete contact information is available at: <https://pubs.acs.org/doi/10.1021/acs.jpca.3c07687>

Notes

The authors declare no competing financial interest.

■ ACKNOWLEDGMENTS

J.M.B. and P.P. acknowledge support from NASA grant 80NSSC22K1167. R.C. acknowledges support from Università degli Studi di Milano under grant PSR2022_DIP_005_R-CONT.

■ REFERENCES

- (1) Galli, D.; Palla, F. The dawn of chemistry. *Annu. Rev. Astron. Astrophys.* **2013**, *51*, 163–206.
- (2) Roueff, E.; Lique, F. Molecular excitation in the interstellar medium: Recent advances in collisional, radiative, and chemical processes. *Chem. Rev.* **2013**, *113*, 8906–8938.
- (3) Zuo, J.; Croft, J. F.; Yao, Q.; Balakrishnan, N.; Guo, H. Full-Dimensional Potential Energy Surface for Ro-vibrationally Inelastic Scattering between H₂ Molecules. *J. Chem. Theor. Comput.* **2021**, *17*, 6747–6756.
- (4) Yang, B.; Zhang, P.; Qu, C.; Wang, X.; Stancil, P.; Bowman, J.; Balakrishnan, N.; McLaughlin, B.; Forrey, R. Full-dimensional quantum dynamics of SiO in collision with H₂. *J. Phys. Chem. A* **2018**, *122*, 1511–1520.
- (5) Yang, B.; Wang, X.; Stancil, P.; Bowman, J.; Balakrishnan, N.; Forrey, R. Full-dimensional quantum dynamics of rovibrationally inelastic scattering between CN and H₂. *J. Chem. Phys.* **2016**, *145*, 224307.

- (6) Yang, B.; Balakrishnan, N.; Zhang, P.; Wang, X.; Bowman, J.; Forrey, R.; Stancil, P. Full-dimensional quantum dynamics of CO in collision with H₂. *J. Chem. Phys.* **2016**, *145*, 034308.
- (7) Yao, Q.; Morita, M.; Xie, C.; Balakrishnan, N.; Guo, H. Globally accurate full-dimensional potential energy surface for H₂+ HCl inelastic scattering. *J. Phys. Chem. A* **2019**, *123*, 6578–6586.
- (8) Bakr, B. W.; Smith, D. G.; Patkowski, K. Highly accurate potential energy surface for the He–H₂ dimer. *J. Chem. Phys.* **2013**, *139*, 144305.
- (9) Trumbo, S. K.; Brown, M. E.; Hand, K. P. Sodium chloride on the surface of Europa. *Sci. Adv.* **2019**, *5*, No. eaaw7123.
- (10) Ginsburg, A.; McGuire, B.; Plambeck, R.; Bally, J.; Goddi, C.; Wright, M. Orion SrcI's disk is salty. *Astrophys. J.* **2019**, *872*, 54.
- (11) Rivera-Valentín, E. G.; Chevrier, V. F.; Soto, A.; Martínez, G. Distribution and habitability of (meta) stable brines on present-day Mars. *Nat. Astron.* **2020**, *4*, 756–761.
- (12) Acharyya, K.; Herbst, E. Sodium-Bearing Species in Interstellar Environments. *44th COSPAR Scientific Assembly*, 2022; Vol. 44, p 2800.
- (13) Dai, D. J.; Ewing, G. E. Induced infrared absorption of H₂, HD, and D₂ physisorbed on NaCl films. *J. Chem. Phys.* **1993**, *98*, 5050–5058.
- (14) Grunwald, M.; Ewing, G. E. A two-dimensional quantum crystal: H₂ on NaCl (100). *J. Chem. Phys.* **1998**, *109*, 4990–4996.
- (15) Heidberg, J.; Voßberg, A.; Hustedt, M.; Thomas, M.; Briquez, S.; Picaud, S.; Girardet, C. Monolayers of ortho-H₂, para-H₂, para-D₂ and normal-H₂ adsorbed on NaCl (001) single crystal surfaces. *J. Chem. Phys.* **1999**, *110*, 2566–2578.
- (16) Heidberg, J.; Gushanskaya, N.; Schönekas, O.; Schwarte, R. Induced infrared spectra of H₂ adsorbed on alkali halide surfaces: separation of ortho-and para-H₂ by desorption. *Surf. Sci.* **1995**, *331*–333, 1473–1478.
- (17) Toennies, J. P.; Traeger, F. The structures and vibrations of H₂ monolayers on NaCl, MgO and LiF: similarities and differences. *J. Phys.: Condens. Matter* **2007**, *19*, 30S009.
- (18) Dawoud, J.; Sallabi, A.; Jack, D. A Monte Carlo simulation study of H₂ layers on NaCl (0 0 1). *Appl. Surf. Sci.* **2008**, *254*, 7807–7811.
- (19) Zhu, Z.; Cao, Y.; Zheng, Z.; Chen, D. An accurate model for estimating H₂ solubility in pure water and aqueous NaCl solutions. *Energies* **2022**, *15*, 5021.
- (20) Anstine, D. M.; Isayev, O. Machine Learning Interatomic Potentials and Long-Range Physics. *J. Phys. Chem. A* **2023**, *127*, 2417–2431.
- (21) Martí, C.; Laganà, A.; Pacifici, L.; Pirani, F.; Coletti, C. A quantum–classical study of the effect of the long range tail of the potential on reactive and inelastic OH+ H₂ dynamics. *Chem. Phys. Lett.* **2021**, *769*, 138404.
- (22) Dörfler, A. D.; Eberle, P.; Koner, D.; Tomza, M.; Meuwly, M.; Willitsch, S. Long-range versus short-range effects in cold molecular ion-neutral collisions. *Nat. Commun.* **2019**, *10*, 5429.
- (23) Grimme, S. Density functional theory with London dispersion corrections. *Wiley Interdiscip. Rev. Comput. Mol. Sci.* **2011**, *1*, 211–228.
- (24) Grimme, S.; Parac, M. Substantial errors from time-dependent density functional theory for the calculation of excited states of large π systems. *ChemPhysChem* **2003**, *4*, 292–295.
- (25) Dreuw, A.; Weisman, J. L.; Head-Gordon, M. Long-range charge-transfer excited states in time-dependent density functional theory require non-local exchange. *J. Chem. Phys.* **2003**, *119*, 2943–2946.
- (26) Stone, A. *The theory of intermolecular forces*; OUP oxford, 2013.
- (27) Zhai, Y.; Caruso, A.; Bore, S. L.; Luo, Z.; Paesani, F. A “short blanket” dilemma for a state-of-the-art neural network potential for water: Reproducing experimental properties or the physics of the underlying many-body interactions? *J. Chem. Phys.* **2023**, *158*, 084111.
- (28) Xia, J.; Zhang, Y.; Jiang, B. Accuracy Assessment of Atomistic Neural Network Potentials: The Impact of Cutoff Radius and Message Passing. *J. Phys. Chem. A* **2023**, *127*, 9874–9883.
- (29) Ko, T. W.; Finkler, J. A.; Goedecker, S.; Behler, J. A fourth-generation high-dimensional neural network potential with accurate electrostatics including non-local charge transfer. *Nat. Commun.* **2021**, *12*, 398.
- (30) Tang, K. T.; Toennies, J. P. An improved simple model for the van der Waals potential based on universal damping functions for the dispersion coefficients. *J. Chem. Phys.* **1984**, *80*, 3726–3741.
- (31) Qu, C.; Yu, Q.; Houston, P. L.; Pandey, P.; Conte, R.; Nandi, A.; Bowman, J. M. Diffusion Monte Carlo and PIMD calculations of radial distribution functions using an updated CCSD (T) potential for CH₅⁺. *Mol. Phys.* **2023**, No. e2262058.
- (32) Nandi, A.; Qu, C.; Houston, P. L.; Conte, R.; Yu, Q.; Bowman, J. M. A CCSD (T)-based 4-body potential for water. *J. Phys. Chem. Lett.* **2021**, *12*, 10318–10324.
- (33) Yu, Q.; Qu, C.; Houston, P. L.; Conte, R.; Nandi, A.; Bowman, J. M. q-AQUA: A Many-Body CCSD(T) Water Potential, Including Four-Body Interactions, Demonstrates the Quantum Nature of Water from Clusters to the Liquid Phase. *J. Phys. Chem. Lett.* **2022**, *13*, 5068–5074.
- (34) Lodi, L.; Tennyson, J.; Polyansky, O. L. A Global, High Accuracy Ab Initio Dipole Moment Surface for the Electronic Ground State of the Water Molecule. *J. Chem. Phys.* **2011**, *135*, 034113.
- (35) Werner, H. J.; Knowles, P. J.; Knizia, G.; Manby, F. R.; Schütz, M. Molpro: a general-purpose quantum chemistry program package. *Wiley Interdiscip. Rev. Comput. Mol. Sci.* **2012**, *2*, 242–253.
- (36) Werner, H. J.; Knowles, P. J.; Manby, F. R.; Black, J. A.; Doll, K.; Heßelmann, A.; Kats, D.; Köhn, A.; Korona, T.; Kreplin, D. A.; et al. The Molpro quantum chemistry package. *J. Chem. Phys.* **2020**, *152*, 144107.
- (37) Kendall, R. A.; Dunning, T. H., Jr.; Harrison, R. J. Electron affinities of the first-row atoms revisited. Systematic basis sets and wave functions. *J. Chem. Phys.* **1992**, *96*, 6796–6806.
- (38) Qu, C.; Conte, R.; Houston, P. L.; Bowman, J. M. Plug and play full-dimensional ab initio potential energy and dipole moment surfaces and anharmonic vibrational analysis for CH₄–H₂O. *Phys. Chem. Chem. Phys.* **2015**, *17*, 8172–8181.
- (39) MSA Software with Gradients, 2019. <https://github.com/szquchen/MSA-2.0>, accessed Jan 1 20, 2019.
- (40) Houston, P. L.; Qu, C.; Yu, Q.; Conte, R.; Nandi, A.; Li, J. K.; Bowman, J. M. PESPIP: Software to fit complex molecular and many-body potential energy surfaces with permutationally invariant polynomials. *J. Chem. Phys.* **2023**, *158*, 044109.
- (41) Xie, Z.; Bowman, J. M. Permutationally invariant polynomial basis for molecular energy surface fitting via monomial symmetrization. *J. Chem. Theor. Comput.* **2010**, *6*, 26–34.
- (42) MSA Software 1.0 with Video, 2016, <https://scholarblogs.emory.edu/bowman/msa/>.
- (43) Wang, Y.; Bowman, J. M.; Kamarchik, E. Five ab initio potential energy and dipole moment surfaces for hydrated NaCl and NaF. I. Two-body interactions. *J. Chem. Phys.* **2016**, *144*, 114311.
- (44) Wolniewicz, L.; Simbotin, I.; Dalgarno, A. Quadrupole transition probabilities for the excited rovibrational states of H₂. *Astrophys. J. Suppl.* **1998**, *115*, 293–313.
- (45) Anderson, J. B. A random-walk simulation of the Schrödinger equation: H₃⁺. *J. Chem. Phys.* **1975**, *63*, 1499–1503.
- (46) Kosztin, I.; Faber, B.; Schulten, K. Introduction to the diffusion Monte Carlo method. *Am. J. Phys.* **1996**, *64*, 633–644.
- (47) McCoy, A. B. Diffusion Monte Carlo Approaches for Investigating the Structure and Vibrational Spectra of Fluxional Systems. *Int. Rev. Phys. Chem.* **2006**, *25*, 77–107.
- (48) Electronic interaction energies of NaCl+H₂. 2023, <https://github.com/jmbowma/QM-22>, accessed Dec 20, 2023.